ELSEVIER

Earth and Planetary Science Letters 160 (1998) 15–30

EPSL

MHD flow in a slightly differentially rotating spherical shell, with conducting inner core, in a dipolar magnetic field

Emmanuel Dormy [a,*], Philippe Cardin [b,c,1], Dominique Jault [a,c]

[a] *IPGP, 4 place Jussieu, F-75252 Paris, France*
[b] *ENS, 24 rue Lhomond, F-75231 Paris, France*
[c] *CNRS, Paris, France*

Received 17 March 1997; revised version received 7 April 1998; accepted 24 April 1998

Abstract

Motion is generated in a rotating spherical shell, by a slight differential rotation of the inner core. We show how the numerical solution tends, with decreasing Ekman number, to the asymptotic limit of Proudman [J. Fluid Mech. 1 (1956) 505–516]. Starting from geophysically large values, we show that the main qualitative features of the asymptotic solution show up only when the Ekman number is decreased below 10^{-6}. Then, we impose a dipolar and force-free magnetic field with internal sources. Both the inner core and the liquid shell are electrically conducting. The first effect of the Lorentz force is to smooth out the change in angular velocity at the tangent cylinder. As the Elsasser number is further increased, the Proudman–Taylor constraint is violated, Ekman layers are changed into Hartmann type layers, shear at the inner sphere boundary vanishes, and the flow tends to a bulk rotation together with the inner sphere. Unexpectedly, for increasing strength of the field, there is a super-rotation (the angular velocity does not reach a maximum at the inner core boundary but in the interior of the fluid) localized in an equatorial torus. At a given field strength, the amplitude of this phenomenon depends on the Ekman number and tends to vanish in the magnetostrophic limit.

Keywords: dynamos; Earth; magnetic field; induction; models

1. Introduction

As we try to model the Earth's dynamo, we face successive difficulties. In particular, the kinematic viscosity of the fluid is very low and this lets other forces dominate viscous diffusion except on very short scales. We hope that the study of some simplified problems will shed light on the numerical difficulties associated with the limit of small Ekman numbers. We present here a study of such a problem, axisymmetric, where all motions are generated by differentially rotating boundaries in the presence of an imposed magnetic field. We will study the steady solution for a wide range of parameters, and try to infer conclusions on the asymptotic limit. The solution involves nice examples of boundary and internal shear layers driven by Ekman pumping and/or Hartmann electric currents.

* Corresponding author. Present address: I.G.P.P. University of California, Los Angeles, CA 90024-1567, USA.
E-mail: dormy@math.ucla.edu
[1] Present address: L.G.I.T., B.P. 53, F-38041 Grenoble, France.

0012-821X/98/$19.00
PII S0012-821X(98)00078-8

For one part (in the absence of a magnetic field), the motivation of this work is to use our three-dimensional convection code on a simple problem, easier to solve, and for which the asymptotic solution is well understood after the work of Proudman [1] and Stewartson [2]. This allows us to test the performances and the limitations of our approach. This problem, though much easier then 3D MHD convection (it is axisymmetric, no heat equation considered), is nevertheless attractive since it possesses a non-trivial solution in the asymptotic limit of vanishing viscosity. Moreover, this problem presents a singularity at the cylinder tangent to the inner core which is a major difficulty for a spherical numerical code to deal with. In this respect, we complete the previous numerical study of Hollerbach [3] restricted to larger Ekman values.

On the other hand, the problem has not been studied before in the presence of a magnetic field and with a conducting inner core. Hopefully, this numerical study may guide future analytical works. Kleeorin et al. [4] have already studied analytically a similar problem, but for an insulating inner core. This makes an important difference but they have been nevertheless able to compare some features of their solution with our numerical findings.

Finally, recent claims of a discovery of a differential rotation of the Earth's inner core [5,6] adds, if necessary, further motivation to understand better the flow between slightly differentially rotating spheres, and the effects of an imposed magnetic field on this flow.

2. Modelling

An incompressible fluid of kinematic viscosity ν, density ρ, magnetic diffusivity η, magnetic permeability μ_0, is enclosed between two spheres. The inner solid body is rotating slightly faster than the outer sphere (Fig. 1). Their rotation rates are, respectively, $(1+\varepsilon)\Omega$ and Ω. The equations are written in the rotating frame where the outer sphere is at rest.

Using the outer sphere radius r_o as length scale, the period of angular rotation of the inner sphere with respect to the outer one $[\varepsilon\Omega]^{-1}$ as unit of time, and the maximum amplitude of the imposed magnetic field $\boldsymbol{B}_0$ at the outer sphere to scale magnetic field $\boldsymbol{B}$,

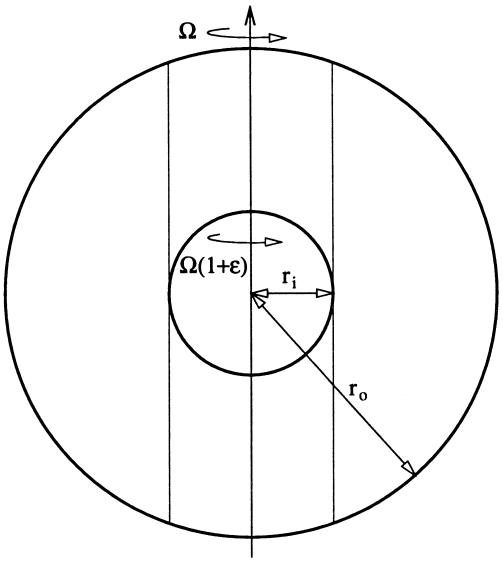

Fig. 1. The geometry of the problem is represented here in a meridional plane. The flow is driven by a slight differential rotation between the inner and the outer spheres, and remains axisymmetric.

the momentum equation and the induction equation write:

$$\begin{cases} \varepsilon\left(\dfrac{\partial \boldsymbol{u}}{\partial t}+\boldsymbol{u}\nabla\,\boldsymbol{u}\right) = -\nabla\pi + E\Delta\boldsymbol{u} - 2\boldsymbol{z}\wedge\boldsymbol{u} \\ \qquad\qquad + \Lambda P_{\mathrm{m}}^{-1}E\varepsilon^{-1}(\nabla\wedge\boldsymbol{B})\wedge\boldsymbol{B} \\ \nabla\cdot\boldsymbol{u} = 0 \\ \dfrac{\partial\boldsymbol{B}}{\partial t} = \nabla\wedge(\boldsymbol{u}\wedge\boldsymbol{B}) \\ \qquad\qquad + P_{\mathrm{m}}^{-1}E\varepsilon^{-1}\Delta\boldsymbol{B} \\ \nabla\cdot\boldsymbol{B} = 0 \end{cases} \tag{1}$$

Where $\boldsymbol{z}$ is the unit vector parallel to the axis of rotation, and the centrifugal acceleration is included in π. The geometry is fully determined by the ratio r_i/r_o which has been kept constant and equal to 0.35 throughout this study. The outer boundary ($r=1$) is insulating and rigid ($\boldsymbol{u}=0$). The inner core has been taken as either insulating or conducting, with the same conductivity as the fluid and $\boldsymbol{u}=s\boldsymbol{e}_\phi$ where (s,ϕ,z) denote cylindrical coordinates. The dimensionless parameters are the Ekman number E, the Elsasser number Λ, and the magnetic Prandtl

number P_m:

$$E = \frac{\nu}{\Omega r_o^2}, \quad \Lambda = \frac{B_0^2}{\Omega \rho \mu \eta}, \quad P_m = \frac{\nu}{\eta} \tag{2}$$

Four dimensionless numbers, ε, E, Λ, P_m are thus necessary to describe the problem.

The computer code is written in such a way that we can investigate the effects of the nonlinear terms $\boldsymbol{u}\nabla\boldsymbol{u}$ and $\nabla \wedge (\boldsymbol{u} \wedge \boldsymbol{B})$. However, these terms play no part in the solution when ε is small enough ($\varepsilon \ll E^{1/3}$). With ε large enough, 3D instabilities are expected [7,8]. This study focuses on the linear solution. Then, the induced perturbation $\boldsymbol{b}$ to the force-free imposed field can be scaled such that:

$$\boldsymbol{B} = \boldsymbol{B}_0 + (\varepsilon P_m E^{-1})\boldsymbol{b} \tag{3}$$

and the system (Eq. 1) reduces to:

$$\begin{cases} \varepsilon \dfrac{\partial \boldsymbol{u}}{\partial t} = -\nabla\pi + E\Delta\boldsymbol{u} - 2\boldsymbol{z} \wedge \boldsymbol{u} \\ \qquad\qquad + \Lambda(\nabla \wedge \boldsymbol{b}) \wedge \boldsymbol{B}_0 \\ \nabla \cdot \boldsymbol{u} = 0 \\ \varepsilon P_m E^{-1} \dfrac{\partial \boldsymbol{b}}{\partial t} = \nabla \wedge (\boldsymbol{u} \wedge \boldsymbol{B}_0) + \Delta\boldsymbol{b} \\ \nabla \cdot \boldsymbol{b} = 0 \end{cases} \tag{4}$$

Two parameters only (E, Λ) fully determine steady state solutions. We have not investigated transient solutions and we have found (covering a large range of parameters E, Λ) that, within this frame (axisymmetric fields and $\varepsilon \ll 1$), the solution always settles down to a steady state.

3. Numerical model

Vector fields are decomposed into poloidal and toroidal parts:

$$\begin{aligned} \boldsymbol{u} &= \nabla \wedge (\nabla \wedge \boldsymbol{r}u_p) + \nabla \wedge \boldsymbol{r}u_t \\ &= \frac{1}{r\sin\theta} \nabla u_{pol} \wedge \boldsymbol{e}_\phi + u_\phi \boldsymbol{e}_\phi \end{aligned} \tag{5}$$

$$\begin{aligned} \boldsymbol{b} &= \nabla \wedge (\nabla \wedge \boldsymbol{r}b_p) + \nabla \wedge \boldsymbol{r}b_t \\ &= \frac{1}{r\sin\theta} \nabla b_{pol} \wedge \boldsymbol{e}_\phi + b_\phi \boldsymbol{e}_\phi \end{aligned} \tag{6}$$

Applying $\boldsymbol{r} \cdot \nabla\wedge$ and $\boldsymbol{r} \cdot \nabla \wedge \nabla\wedge$ to Eq.4 ,w e get the set of scalar equations:

$$\begin{cases} \varepsilon \dfrac{\partial}{\partial t} L_2 u_t = E\Delta L_2 u_t + 2(\boldsymbol{z} \wedge \boldsymbol{r} \cdot \nabla)u_t - 2Qu_p \\ \qquad\qquad + \Lambda \boldsymbol{r} \cdot \nabla \wedge [(\nabla \wedge \boldsymbol{b}) \wedge \boldsymbol{B}_0] \\ \varepsilon \dfrac{\partial}{\partial t} L_2 \Delta u_p = E L_2 \Delta^2 u_p + 2(\boldsymbol{z} \wedge \boldsymbol{r} \cdot \nabla)\Delta u_p \\ \qquad\qquad + 2Qu_t - \Lambda \boldsymbol{r} \cdot \nabla \wedge \nabla \\ \qquad\qquad \wedge [(\nabla \wedge \boldsymbol{b}) \wedge \boldsymbol{B}_0] \\ \varepsilon \dfrac{P_m}{E} \dfrac{\partial}{\partial t} L_2 b_t = \Delta L_2 b_t + \boldsymbol{r} \cdot \nabla \wedge [\nabla \wedge (\boldsymbol{u} \wedge \boldsymbol{B}_0)] \\ \varepsilon \dfrac{P_m}{E} \dfrac{\partial}{\partial t} L_2 b_p = \Delta L_2 b_p + \boldsymbol{r} \cdot \nabla \wedge (\boldsymbol{u} \wedge \boldsymbol{B}_0) \end{cases} \tag{7}$$

where L_2 is the Beltrami operator

$$\begin{aligned} L_2 &= \frac{\partial}{\partial r} r^2 \frac{\partial}{\partial r} - r^2\Delta \\ &= -\frac{1}{\sin\theta} \frac{\partial}{\partial\theta} - \frac{1}{\sin^2\theta} \frac{\partial^2}{\partial\phi^2} \end{aligned} \tag{8}$$

and Q (introduced in Roberts [9]) is the operator defined as:

$$Q = \boldsymbol{z} \cdot \nabla - \tfrac{1}{2}(L_2 \boldsymbol{z} \cdot \nabla + \boldsymbol{z} \cdot \nabla L_2) \tag{9}$$

The scalar u_t, u_p, b_t, b_p are decomposed as:

$$X = \sum_l x_l(r) Y_l^0 \tag{10}$$

where $x_l(r)$ is sampled at discrete points. The cross products with $\boldsymbol{B}_0$ terms are computed in the physical space on Gauss collocation points, and are re-integrated in the spectral space. Vertical discretization is achieved using a Finite Difference scheme on a non-uniform grid stretched in the vicinity of the boundaries. It required 3000 shells to resolve the structures corresponding to an Ekman number of 10^{-8}. Eq. 7 is time stepped until the solution changes very little. Time integration is performed using a Crank–Nicholson scheme for diffusion terms, and an Adams–Bashforth scheme for other terms. Hence, the calculation of the diffusion term in each of Eq. 7 requires a product and an inversion of either 3- or 5-banded diagonal matrix at each time step.

4. Solution in the non-magnetic case

In a first step, we study how the solution in the non-magnetic case depends on the Ekman number E and we recover the asymptotic solution of Proudman and Stewartson [1,2].

4.1. Ekman layers

The numerical study of Ekman layers raises important problems that can be partly alleviated by using a radial grid, which is stretched in the vicinity of the two boundaries. It is essential to determine how many points are needed to resolve these viscous layers properly. Another difficulty is due to the steep gradient of the solution in these layers. Spurious oscillations often arise in the vicinity of shear layers; it is difficult to ensure that they are kept small, that they do not spoil the solution (they do not blow up), and that they do disappear in the steady state regime after time integration of transient states. Around ten points, in the layer, are found to be needed (if regularly spaced) to resolve the structure correctly with our finite difference scheme. When only three points are used, the structure of the layer is not properly solved, the calculated suction is erroneous, and this has important consequences on the main flow computed outside the layer, as can be seen on Fig. 2.

4.2. The Proudman–Stewartson solution

The problem we consider is strongly dominated by rotation. In the limit of small viscosity, all motions in the interior should satisfy the Proudman–Taylor theorem (vertically invariant flow):

$$\boldsymbol{u} = u_\phi(s)\boldsymbol{e}_\phi + \frac{1}{s}\nabla u_{\rm pol}(s) \wedge \boldsymbol{e}_\phi \tag{11}$$

The cylindrical surface that touches the inner sphere (the axis being the axis of rotation) will be referred to as the tangent cylinder. Outside the tangent cylinder, the asymptotic state is rigid rotation with the same angular velocity as the outer sphere:

$$u_\phi(s) = u_{\rm pol}(s) = 0 \tag{12}$$

Inside the tangent cylinder the angular velocity of geostrophic cylinders in the asymptotic regime is determined by the Proudman constraint in the volume and by Ekman pumping at the boundaries [1]:

$$u_\phi(s) = \frac{s(1-s^2)^{1/4}}{(1-s^2)^{1/4} + [1-(s/r_{\rm i})^2]^{1/4}} \tag{13}$$

$$u_{\rm pol}(s) = \frac{E^{1/2}s^2}{2\{(1-s^2)^{1/4} + [1-(s/r_{\rm i})^2]^{1/4}\}} \tag{14}$$

where the notations of Proudman are related to ours by:

$$\psi' = u_{\rm pol}, \quad \xi' = s u_\phi \tag{15}$$

The resulting cylindrical shear layer was investigated by Stewartson [2] who proved that it does not exert a control on the interior flow. This layer allows the flow to recirculate from one Ekman layer to the other and also accommodates the jump in azimuthal velocity. Stewartson showed that the shear layer can be divided into three nested layers. In the two outer layers, the z-dependence of u_ϕ may be neglected and interior viscous stresses on the cylinders balance viscous stresses on the boundaries. As a consequence, $u_{\rm pol}$ depends on z, as can be seen from the ϕ component of the momentum equation. For $s > r_{\rm i}$, the width of the layer is $O(E^{1/4})$ and both u_ϕ and $u_{\rm pol}$ decrease exponentially to zero. For $s < r_{\rm i}$, the width of the layer is $O(E^{2/7})$ and the s-dependence of the solution is given by Bessel and Gamma functions. The remaining discontinuity in $u_{\rm pol}$ is removed in the inner layer of width $O(E^{1/3})$. This layer is fully ageostrophic. Stewartson's analysis is well illustrated by the numerical study.

4.3. Numerical study

The solutions are calculated for different Ekman numbers. As the Ekman number is decreased, the singularity on the tangent cylinder develops, and more and more harmonics are required to represent the associated fields. Harmonics up to degree 1300 were needed to compute the solution for $E = 10^{-8}$. If one was to use fewer harmonics, this would lead to oscillations comparable to Gibbs phenomenon (see Morse and Feshbach [11]).

The results published by Hollerbach [3], for Ekman numbers $E_{\rm H} \geq 10^{-5}$ are reproduced (Fig. 3). We note that his Ekman number $E_{\rm H}$ is related to ours by:

$$E_{\rm H} = 2.37E \tag{16}$$

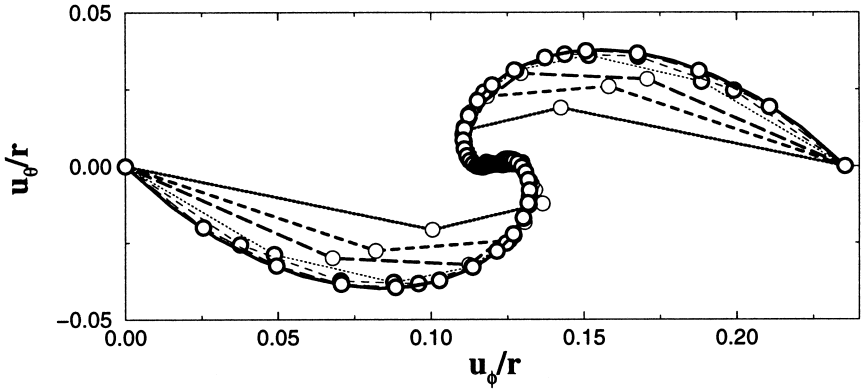

Fig. 2. Ekman spirals. u_θ/r versus u_ϕ/r for different number of grid points. $\theta = \pi/12$, $E = 10^{-5}$. These results compare very well with the linear theory [10].

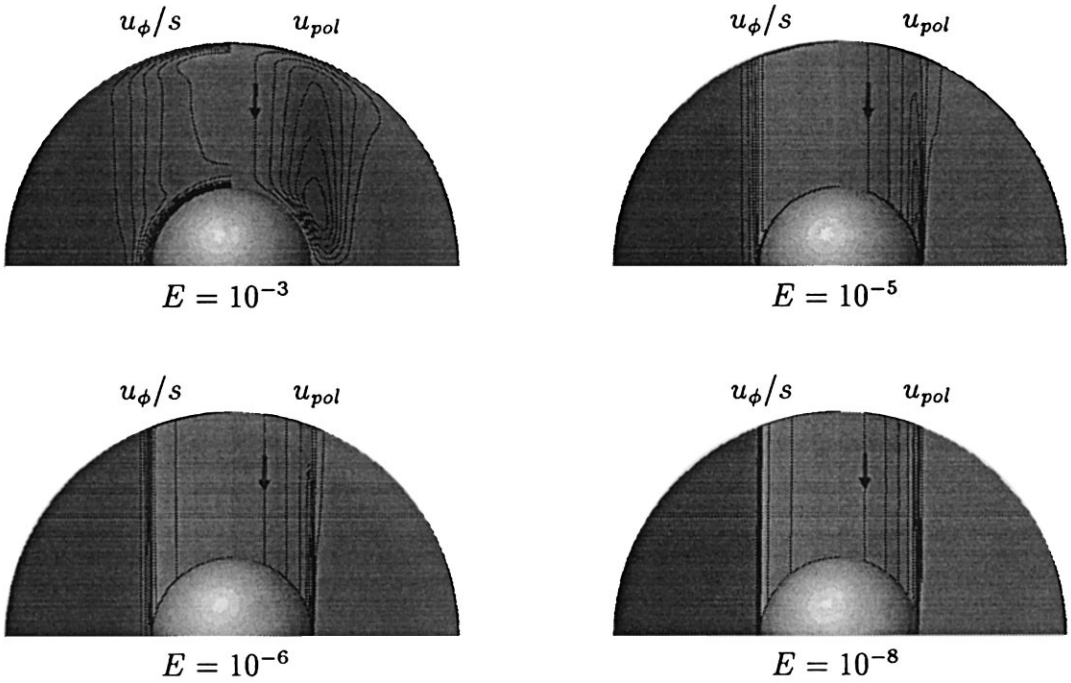

Fig. 3. Meridional section of angular velocity and $u_{\rm pol}$ for decreasing values of the Ekman number. First two figures compare very well with fig. 3 of [3]. The qualitative asymptotic behavior of flow synchronization with the inner core rotation close to $s = 0.35$ can be observed only on the two last figures.

We have recovered the interior geostrophic solution found by Proudman [1]. The meridional flow scales as $O(E^{1/2})$. The asymptotic behaviour of flow synchronization with the inner core rotation, as the tangent cylinder is approached, can be qualitatively observed only when $E \leq 10^{-6}$ (see Fig. 4). We have showed u_ϕ/s and $u_{\rm pol}$ as a function of z and r whereas we are, of course, interested by the (s,z)-structure of the solution; numerical convenience dictated our choice.

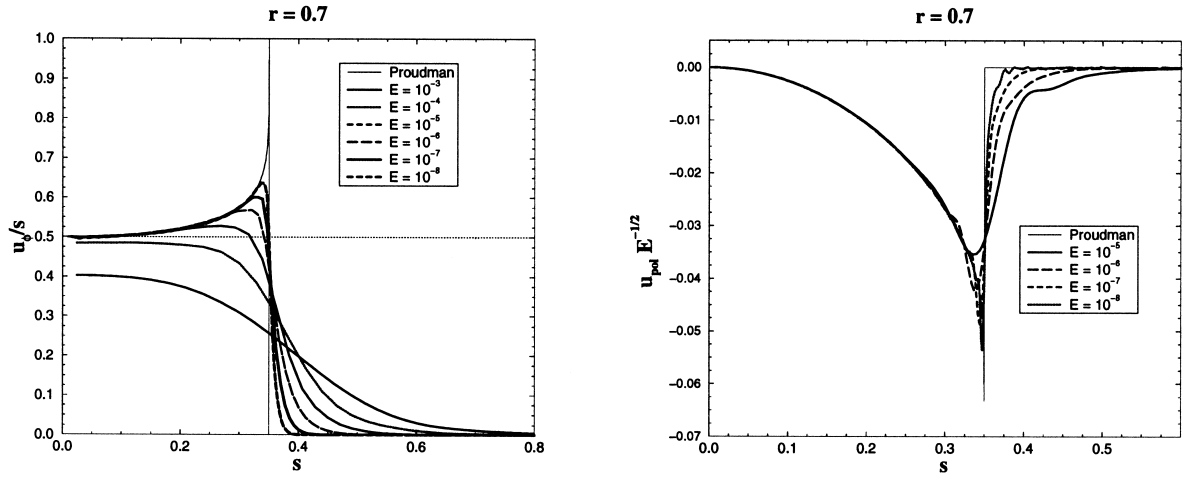

Fig. 4. Comparison with the Proudman solution. Angular velocity u_ϕ/s and poloidal scalar $u_{\rm pol}E^{1/2}$ versus s at $r = 0.7$ for different Ekman numbers. The Proudman solution is shown with a thin solid line. The angular velocity solutions for $E > 10^{-6}$ do not show the qualitative behavior of the asymptotic limit.

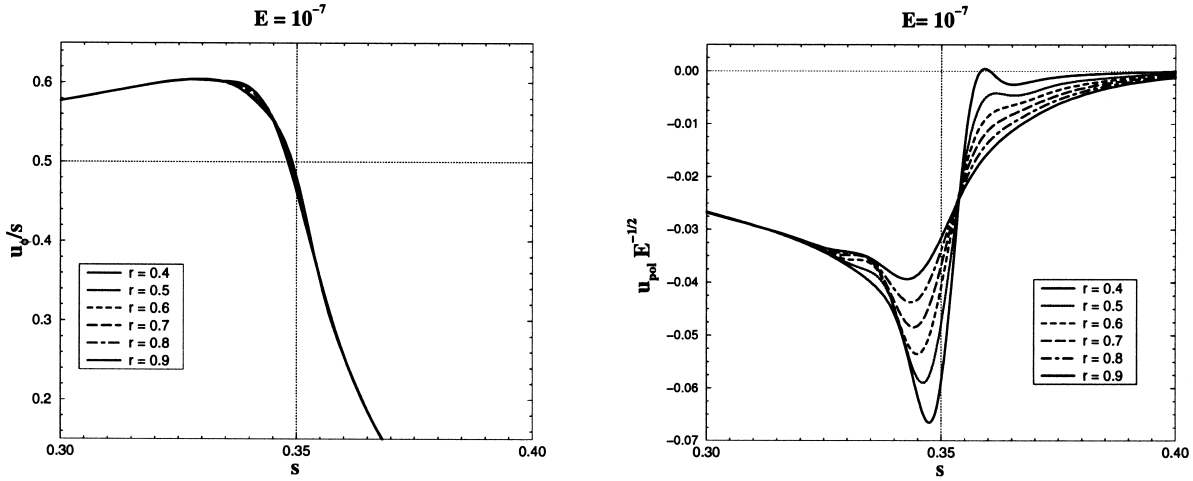

Fig. 5. Comparison with the Stewartson asymptotics. Angular velocity u_ϕ/s and poloidal field $u_{\rm pol}E^{1/2}$ versus s for different radius r. The inner ageostrophic layer of width $E^{1/3}$ is well distinguished from the outer layers where the azimuthal flow is geostrophic.

We can also study the departure from the Proudman solution in the cylindrical shear layer. Fig. 5 illustrates well the three nested layers. The inner layer of width $O(E^{1/3})$, where u_ϕ is ageostrophic, is well defined and is clearly embedded in the outer shear layers, where u_ϕ is z-independent but $u_{\rm pol}$ depends on z. The transport of fluid takes place at small z inside the tangent cylinder and at large z outside the tangent cylinder (see also Fig. 3). We have calculated the rate of exponential decrease of u_ϕ and $u_{\rm pol}$ with s for $(s > r_{\rm i})$ (Table 1). The agreement with the $E^{1/4}$ scaling of Stewartson is gratifying. In order to investigate the outer layers, we have subtracted the mainstream solution (Eqs. 13 and 14). Furthermore, we have stretched the s coordinate by the factor $E^{-2/7}$, for $s < r_{\rm i}$, and by the factor $E^{-1/4}$, for $s > r_{\rm i}$. The $O(E^{2/7})$ and $O(E^{1/4})$ scalings are vindicated (Fig. 6) inasmuch as the mainstream solution is

Table 1
$E^{1/3}$ and $E^{1/4}$ Stewartson layers

E	δ	λ_1	λ_2
10^{-5}	0.117	−23.02	19.5
10^{-6}	0.057	−38.41	33.89
10^{-7}	0.027	−73.40	63.94
10^{-8}	0.013	−129.52	106.71
	$E^{-0.32}$	$E^{-0.253}$	$E^{-0.249}$

δ is the width of the region where u_ϕ is ageostrophic. λ_1 and λ_2 are the rate of exponential decrease of, respectively, u_ϕ and $u_{\rm pol}$ outside the tangent cylinder. The last line gives the slope of the regression of these coefficients on $\log E$.

recovered for a fixed distance to the tangent cylinder. However, the influence of the $O(E^{1/3})$ layer on $u_{\rm pol}$ inside the tangent cylinder is also visible. Stretching now the s coordinate by $E^{-1/3}$, we characterize further the $O(E^{1/3})$ layer, whose influence on $u_{\rm pol}$ is the strongest at small z (Fig. 7): the maxima are now aligned at a fixed distance to the tangent cylinder. Finally, Fig. 8 demonstrates that the width of the layer where u_ϕ is ageostrophic scales with $E^{1/3}$ (see also Table 1) as predicted by Stewartson [2].

The scaling laws given by Stewartson apply well to the numerical solution for the range of Ekman numbers $[10^{-6}, 10^{-8}]$, even if some features of the Stewartson solution are absent from the numerical solution. As an example, the amplitude of $E^{-1/2}u_{\rm pol}$ increases rapidly with E^{-1} in the $E^{-1/3}$ inner layer (cf. Fig. 7), whereas Stewartson [2] predicted very slow variation ($E^{-1/21}$). We note also that the z-dependence of $u_{\rm pol}$ in the $E^{2/7}$ layer out of the $E^{1/3}$ inner layer is not linear as predicted (Fig. 5).

5. Magnetohydrodynamics

We now study how the flow is modified in the presence of an imposed magnetic field (Fig. 9).

5.1. The imposed magnetic field

Only current-free fields have been investigated ($J = 0$). A current free field with external sources, when axisymmetric and dipolar, is aligned along the axis of rotation. As a consequence, shear at the tangent cylinder does not create electric currents. We have checked that, in this case, the shear at the tangent cylinder is not reduced by magnetic effects, and is even reinforced for strong fields, as the Lorentz force efficiently couples the fluid inside the tangent cylinder with the inner sphere. The asymptotic solution for large Λ consists of bulk rotation of the fluid volume inside the tangent cylinder together with the inner body and a bulk rotation of the fluid volume exterior to the cylinder together with the outer sphere (see also the recent study by Hollerbach [12]).

The problem is very different if the sources of the magnetic field are internal. For the imposed field one

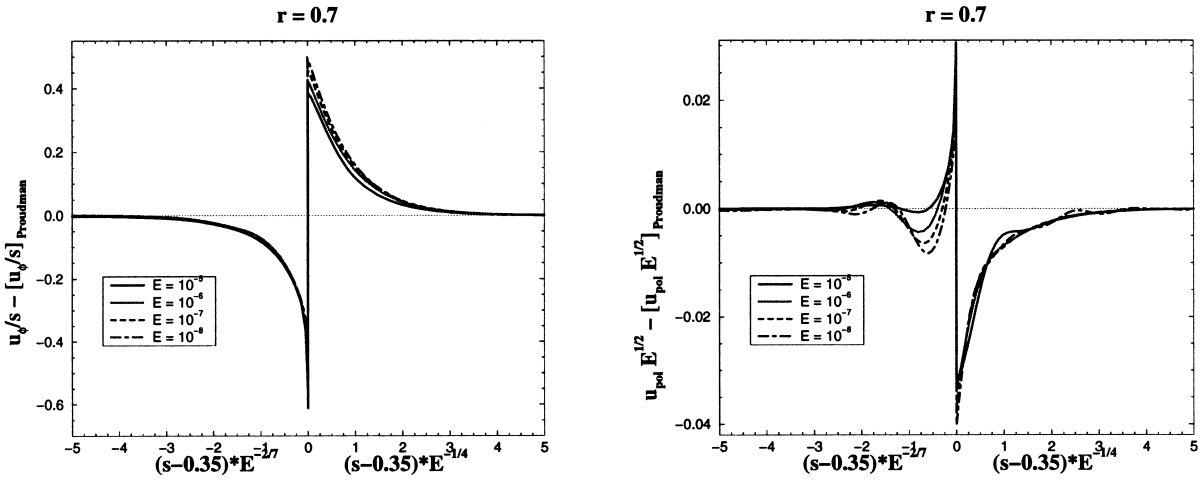

Fig. 6. The outer Stewartson layers. u_ϕ/s and $u_{\rm pol}E^{1/2}$ versus $E^{-2/7}(s-0.35)$ for $s < 0.35$ and $E^{-1/4}(s-0.35)$ for $s > 0.35$ $r = 0.7$.

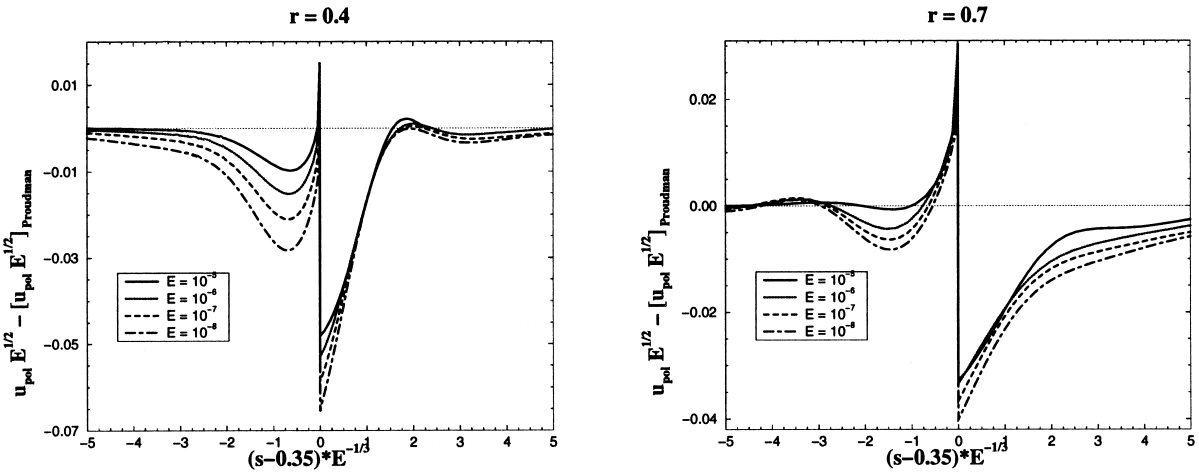

Fig. 7. The inner Stewartson layer. $u_{\rm pol}E^{1/2}$ versus $E^{-1/3}(s-0.35)$. $r=0.4$ (left) and $r=0.7$ (right).

then writes:

$$B_r=\frac{1}{r^3}\cos\theta,\quad B_\theta=\frac{1}{2r^3}\sin\theta \tag{17}$$

Here the magnetic field is not aligned along the axis of rotation, and will therefore cross the tangent cylinder. Important, too, is the variation of the field's magnitude: in this case the amplitude of the field, varying as r^{-3}, will be much stronger at the inner boundary. The field amplitude is 23 times larger at the inner sphere surface than at the boundary with the outer sphere. The local Elsasser number is thus 544 times greater than the value that we quote and calculate with the field at the outer boundary.

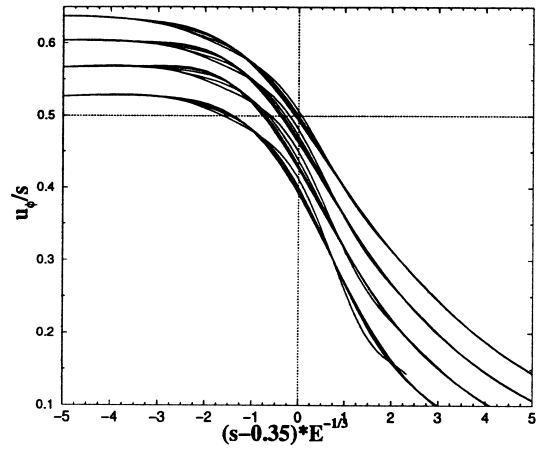

Fig. 8. The inner Stewartson layer. u_ϕ/s versus $E^{-1/3}(s-0.35)$ for different Ekman numbers ($E=10^{-5}$, 10^{-6}, 10^{-7}, 10^{-8} from top to bottom) and different radius ($r=0.4$, 0.5, 0.6, 0.7, 0.8, 0.9).

5.2. Comparison with previous studies and numerical tests

We present results obtained in the case of an insulating inner core in order to compare with the numerical study of Hollerbach [3]. The first effect of the magnetic force is to reduce the shear at the tangent cylinder. As the Elsasser number is increased the motion reduces to a rigid rotation with the outer sphere. Since both spheres are insulating, only viscous torques couple the solid boundaries. Fig. 10 shows how the solution evolves with increasing values of Λ at $E=10^{-5}$. First, we see (for $\Lambda=0$) the influence of the equatorial Ekman layer of width $E^{2/5}$ attached to the inner sphere. Comparison with [3] validates our code. The recent asymptotic study

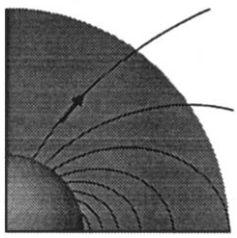

Fig. 9. The imposed magnetic induction.

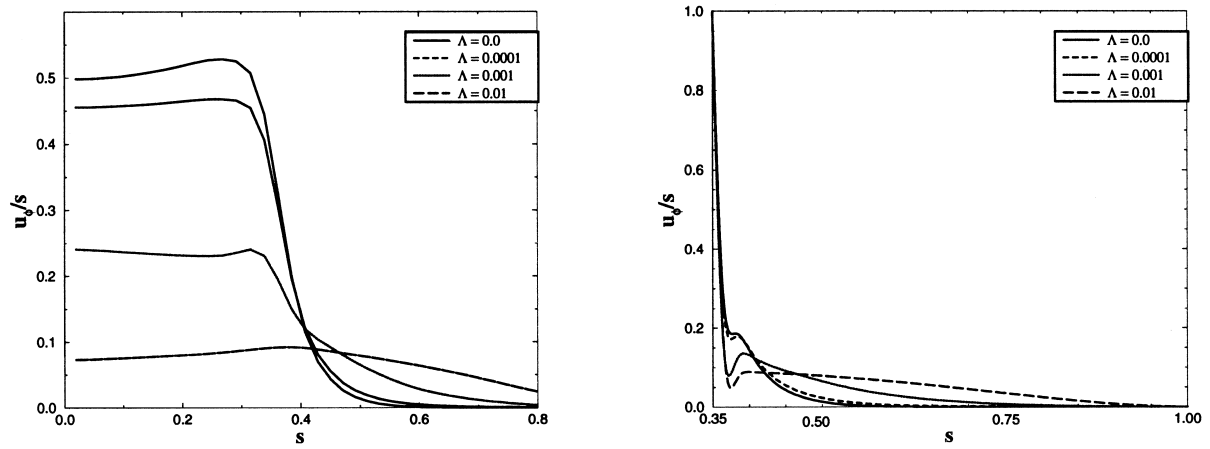

Fig. 10. Angular velocity with respect to the cylindrical radius s in the case of an insulating inner body; on the left hand side at $r = 0.75$, on the right hand side in an equatorial section. $E = 10^{-5}$.

of Kleeorin et al. [4] predicts a local minimum in angular velocity, in the vicinity of the equator of the inner body, in their strong field limit. The reversed flow can be seen on Fig. 10 (see the equatorial section). We note that they refer to a first version of our paper, in which the figures were numbered differently. Fig. 10 was referred to as Fig. 6.

We now restore finite conductivity to the inner core. The induction equation (its diffusive part) must now be solved inside the inner core, also. For non-zero Elsasser numbers, a magnetic torque applies on the inner boundary:

$$\Gamma_B = \Lambda r \iint \boldsymbol{B}_r \boldsymbol{b}_\phi \sin\theta \, \mathrm{d}\boldsymbol{S} \tag{18}$$

Viscous torques act at both boundaries and are expressed as:

$$\Gamma_\nu = Er \iint \sin\theta \boldsymbol{r} \frac{\partial}{\partial \boldsymbol{r}} \frac{\boldsymbol{u}_\phi}{\boldsymbol{r}} \, \mathrm{d}\boldsymbol{S} \tag{19}$$

Equilibrium between these torques is an additional check of our numerical calculation. They agree to within 1%.

5.3. The asymptotic state

We shall see that including a conducting inner core endows the solution with a rich variety of features. When the imposed magnetic field is strong enough, we again expect the solution to be close to a state of rigid rotation. But, now, the internal magnetic torque couples far more efficiently the fluid with the inner body than the external viscous torque with the outer body. As a consequence, most viscous effects are confined to the boundary layer attached to the outer sphere.

5.3.1. Ekman–Hartmann boundary layer

As the Elsasser number is increased from zero to $O(1)$ values, the Ekman boundary layer attached to the outer sphere gradually changes into an Hartmann type boundary layer. Boundary layers influenced by both rotation and magnetic field are reviewed by Acheson and Hide [13]. They give (in their section 5.2) a local derivation of the effect of the boundary layer on the flow and the magnetic field in the interior region when the boundary is insulating. With $\Lambda = 0$, the effect on the flow reduces to the Ekman suction. In the Hartmann limit, the normal component of $\boldsymbol{u}$ vanishes at the edge of the interior region. In between, elimination of the main flow vorticity in the expressions for u_r and j_r yields:

$$\frac{[j_r]}{[u_r]} = \frac{(\boldsymbol{B_0} \cdot \boldsymbol{r})}{B_0} \left(\left(1 + \Lambda_\perp^2\right)^{1/2} + \Lambda_\perp \right) \tag{20}$$

where $[\cdot]$ denotes jump across the boundary layer and $\Lambda_\perp$ is defined as:

$$\Lambda_\perp = \frac{1}{2\boldsymbol{z} \cdot \boldsymbol{r}} \frac{(\boldsymbol{B_0} \cdot \boldsymbol{r})^2}{B_0^2} \Lambda \tag{21}$$

Fig. 11 shows how the Ekman spirals on both boundaries are modified by magnetic effects. The

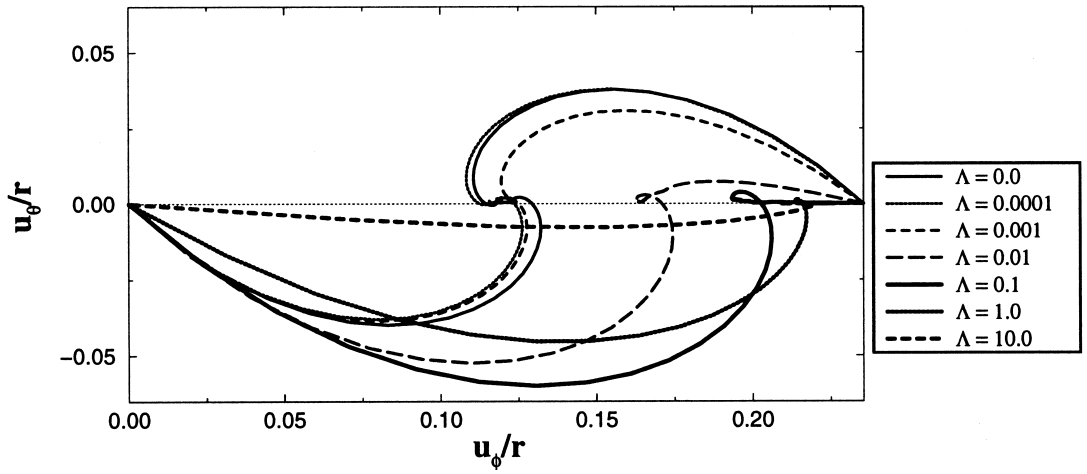

Fig. 11. Same as Fig. 2 in the presence of a magnetic field. As the Elsasser number increases, the angular velocity of the main flow approaches the angular velocity of the inner body. The θ-component of the velocity vanishes as the layers modify from Ekman type to Hartmann type.

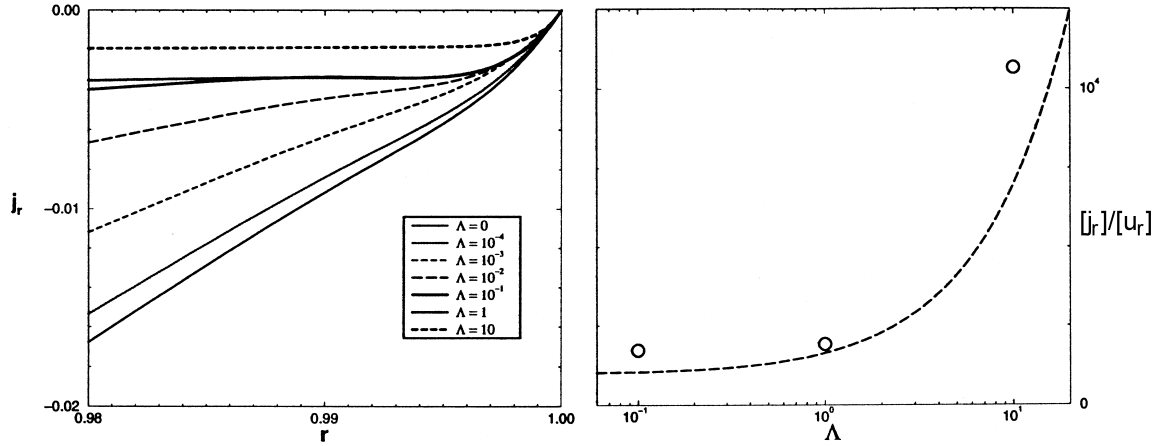

Fig. 12. The outer boundary layer for $E = 10^{-5}$ and $\theta = \pi/12$. On the left hand side, the radial electric current j_r. The current boundary layer is well characterized only for $\Lambda \geq 0.1$. On the right hand side, numerical ($\circ$) and theoretical (as given by Eq. 20) values for $[j_r]/[u_r]$ are represented.

meridional motion u_θ characteristic of the secondary flow in the Ekman layer is reduced and then suppressed as the local Elsasser number is increased to order one. Fig. 12 gives a comparison between Eq. 20 and our numerical results, for $E = 10^{-5}$ with increasing Λ at $\theta = \pi/12$.

5.3.2. *Electric currents ejected from the Hartmann layer*

In this section, we investigate the solution in the limit of large Elsasser numbers: the Hartmann limit. The flow is close to a state of rigid rotation and the main feature of the solution is a Hartmann boundary layer attached to the outer sphere through which the flow velocity decreases from $\sin\theta$ to 0.

We rescale the set of Eq. 4, retaining only the magnetic and viscous forces, and introducing the Hartmann number $M = (\Lambda/E)^{1/2}$. Only one parameter controls the system in this regime. Taking into account the geometry of the imposed field, and introducing $\xi = M(1 - r)$ as radial boundary-layer

coordinate, we get:

$$\begin{cases} \dfrac{\partial^2 \boldsymbol{u}}{\partial \xi^2} - 2\cos\theta \dfrac{\partial \boldsymbol{b}}{\partial \xi} = 0 \\ \dfrac{\partial^2 \boldsymbol{b}}{\partial \xi^2} - 2\cos\theta \dfrac{\partial \boldsymbol{u}}{\partial \xi} = 0 \end{cases} \tag{22}$$

of which the solution is [14]:

$$\boldsymbol{u} = -\boldsymbol{b} = \sin\theta \left(1 - \mathrm{e}^{-2\cos\theta\xi}\right) \tag{23}$$

To ensure $\boldsymbol{j} \wedge \boldsymbol{B} = 0$, $\boldsymbol{b}$ has to be written:

$$\boldsymbol{b} = \frac{1}{r\sin\theta} f\left(\frac{\sin^2\theta}{r}\right) \tag{24}$$

Hence Eq. 23 is compatible with the bulk rotation that we have assumed as solution for the interior flow if:

$$\boldsymbol{b} = \frac{\sin\theta}{r^2} \tag{25}$$

The equations are singular at the equator, where the magnetic field lines are parallel to the boundary.

5.3.3. The equatorial singularity

The singularity of the Hartmann layer has important consequences because it can be shown that the flux of electric currents leaving the boundary layer there does not vanish. We have not pushed the analytical study further (see Roberts [14] for a thorough investigation of such singularities) and we rely here on the numerical study to describe how the equatorial singularity affects the interior flow.

In the presence of rotation forces, the viscous layer is of Ekman type. It is also singular at the equator, where the rotation vector is parallel to the boundary. Numerical study seems necessary to unravel how rotational forces modify the Hartmann solution.

5.4. Numerical study

Fig. 13 illustrates how the flow synchronizes with the inner body as the Elsasser number is increased. For low Elsasser numbers, the electric currents are generated at the inner core and at the tangent cylinder whereas for larger values they are induced by the viscous shear at the outer boundary (see Fig. 14). For large Elsasser numbers, the numerical solution illustrates the role of the equatorial singularity. At high latitude, the electric currents flow along the lines of the imposed dipolar field. In the viscous boundary layer, they converge toward the outer equator and coming back to the inner core, they cross magnetic field lines which are parallel to the outer boundary. Indeed, the magnetic field and the electric field do not share the same symmetry with respect to the equatorial plane. This discrepancy between the symmetries of the two fields holds also in the intermediate regime where electric currents are induced by the remaining shear in the interior region. As a consequence, in the vicinity of the equatorial plane, magnetic forces do not vanish and make the interior flow depart from a state of rigid rotation. Fig. 15 shows the profile of the angular velocity in the equatorial plane for different strengths of the imposed magnetic field at $E = 10^{-5}$. The case $\Lambda = 10$ ($M = 10^3$) exemplifies departure from rigid rotation. Angular velocity reaches a maximum in the interior region. This maximum is still more pronounced at smaller Elsasser number (see $\Lambda = 0.1$, i.e. $M = 10^2$). The accelerated flow closely follows magnetic field lines. With increasing Elsasser number, the peak angular velocity migrates from the inner boundary to the outer sphere and the flow approaches a state of rigid rotation.

In order to better understand how the interior flow is accelerated, we have studied the magneto-viscous equilibrium, where the Coriolis forces are absent (see Figs. 16 and 17). As in Section 5.3.2, the system (Eq. 4) is rescaled so that the Coriolis force is eliminated in the limit $\Lambda \to \infty$, $E \to \infty$ and the remaining dimensionless number, the Hartmann number $M = (\Lambda/E)^{1/2}$ finite. Viscous shear (mainly in the outer boundary layer) generates electric Hartmann currents in the equatorial region crossing the magnetic field lines as described above. Super-rotation of the fluid is thus a magneto-viscous effect. Here, viscous forces only oppose the acceleration of the zonal flow in the equatorial region. The region of accelerated fluid has a banana shape centred on a magnetic field line. The maximum speed grows with increasing Hartmann number, in strong contrast with what is described above. Whereas a weak magnetic field ($M = 1$) changes the dynamics only slightly, a moderate magnetic field ($M = 3.16$) suffices to accelerate the equatorial interior flow. At $M = 316$ and $M = 1000$, the shear is well confined to the bound-

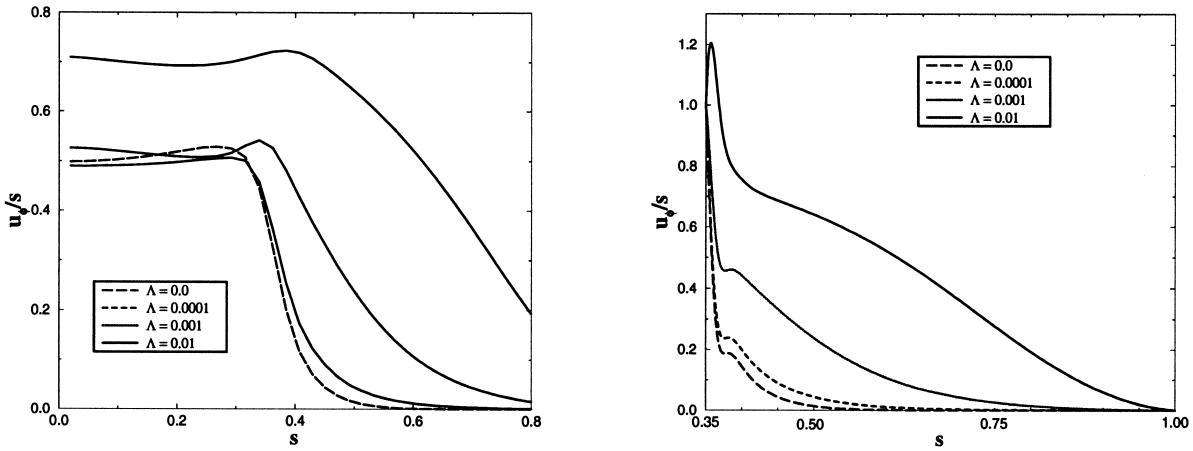

Fig. 13. Angular velocity with respect to the cylindrical radius s in the case of an conducting inner body; on the left hand side at $r = 0.75$ on the right hand side in an equatorial section. Ekman number is 10^{-5}.

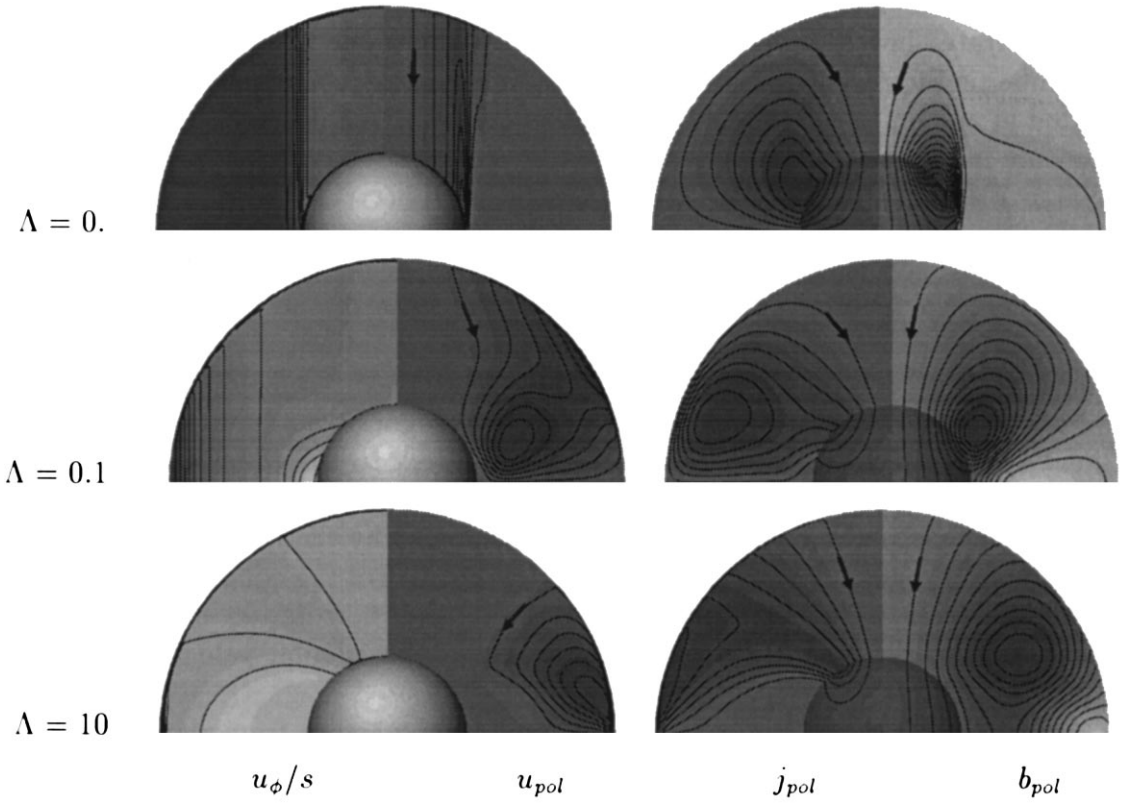

Fig. 14. Meridional sections for $E = 10^{-5}$, and increasing values of the Elsasser number.

ary layer parallel to the magnetic field line tangent to the outer sphere. The width of the sheared zone follows the $M^{-1/2}$ asymptotic law for boundary layer attached to a wall parallel to the imposed magnetic field [15]. This internal shear layer is associated with the recirculation of electric currents induced in the

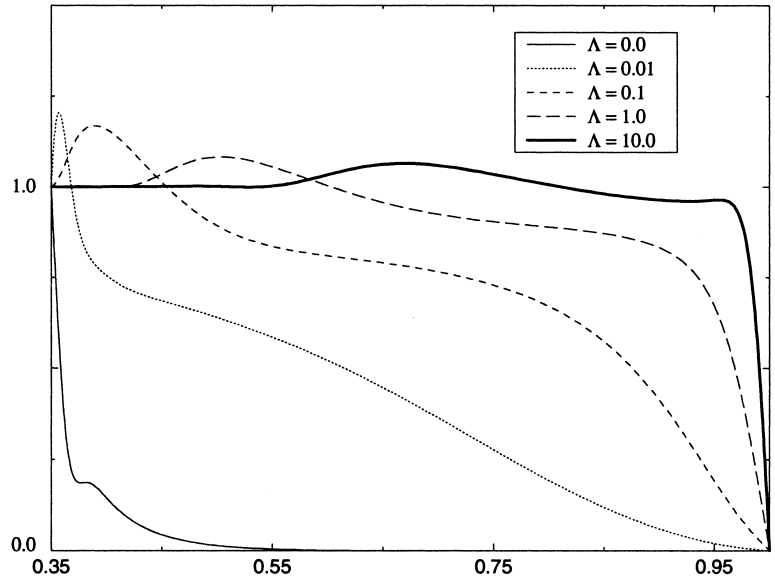

Fig. 15. Equatorial section of angular velocity at Ekman 10^{-5}. As the Elsasser number increases the flow synchronizes with the inner body. Unexpectedly the angular velocity of the flow locally exceeds the outer body's angular velocity.

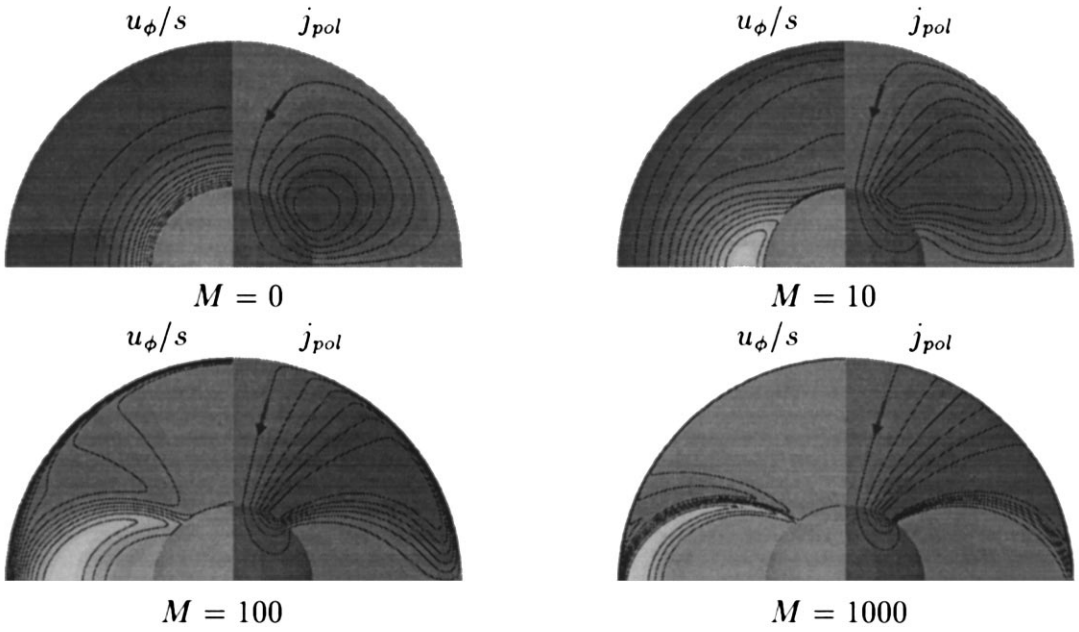

Fig. 16. Meridional representations of the zonal angular velocity u_ϕ/s and the meridional electric currents $j_{\rm pol}$ in the absence of rotational forces for increasing Hartmann numbers.

Hartmann layer as the internal Stewartson layer is associated with the recirculation of the meridional flow generated in the Ekman layers.

Comparison of the solutions with and without the rotational forces shows that they strongly inhibit the equatorial acceleration, which violates

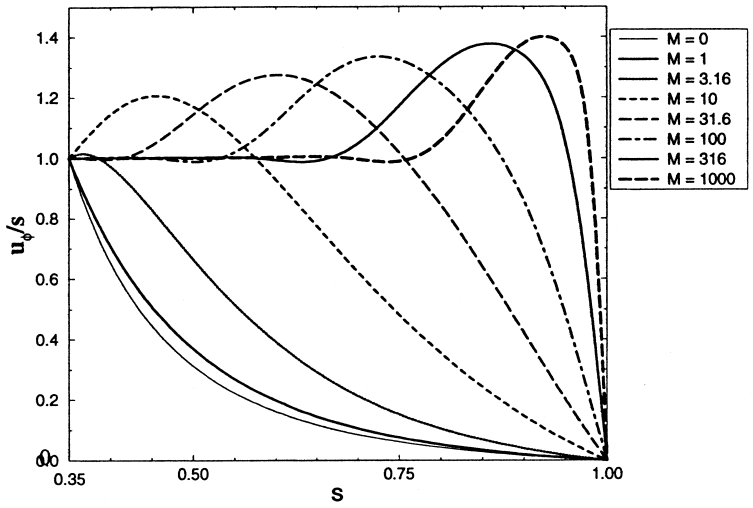

Fig. 17. Equatorial section of the angular velocity in the absence of rotational forces.

the Proudman–Taylor constraint. Besides, departure from a state of rigid rotation is less and less pronounced as viscosity is decreased (see Fig. 18). Decreasing the viscosity indeed restores the role of rotation forces, even for large Elsasser numbers.

Kleeorin et al. [4] have studied how geostrophic velocity (see Fig. 14) reduces to zero as the equator of the outer sphere is approached in the intermediate and strong field limit $E^{1/2} \ll \Lambda \ll 1$. They write the 'modified Taylor's constraint', balance between Maxwell stress in the mainstream flow and the viscous stress in the Ekman–Hartmann boundary layer. They describe a magnetic Proudman layer of width $E^{2/7}/\Lambda^{4/7}$ where viscous stress is negligible except at the top and bottom of the geostrophic cylinders. The remaining discontinuity in the geostrophic velocity is smoothed out in the viscous Stewartson $E^{2/5}$ layer attached to the equator. Kleeorin et al. [4] have compared their result with our numerical work. We note that figs. 12, 13 and 16 of that paper are now, respectively, Figs. 14, 15 and 18. Their table 2 gives the distance in our units from the outer sphere at which the rotation rate is one half the value outside the magnetic Proudman layer, according to their asymptotic theory. Only for $\Lambda = 0.1$, the $E^{2/5}$ Stewartson layer is thin compared to the magnetic Proudman layer. But the agreement between the theoretical and numerical works is striking and vindicates their analytical work.

Finally, the conducting inner body strongly influences the geometry of the electric currents. Electric currents can enter the inner body (because it is conducting) without shearing it (because it is rigid). Fig. 14 shows how the electric currents try to follow the magnetic field lines in the fluid all the way to the inner solid body where they loop back.

6. Conclusion

Very small values of the Ekman number have to be studied in order to get some insight into the asymptotic limit with a numerical study. Ekman numbers such as 10^{-5} are not small enough to describe even qualitatively the asymptotic regime, well-known in the non-magnetic case, and this conclusion holds also with strong magnetic effects. It would be helpful to develop a numerical algorithm to solve the thin boundary layers without increasing the number of grid points too much. The method used here limits the (axisymmetric) studies to E larger than 10^{-8} on some of the fastest computers available.

A new structure, defined as a maximum in the angular rotation inside the interior flow, arises in the equatorial region in the presence of an imposed field. It is present only when the solid inner body is conducting because, firstly, the main boundary layer is attached at the outer sphere and, secondly, the electric currents can loop in the inner body. This

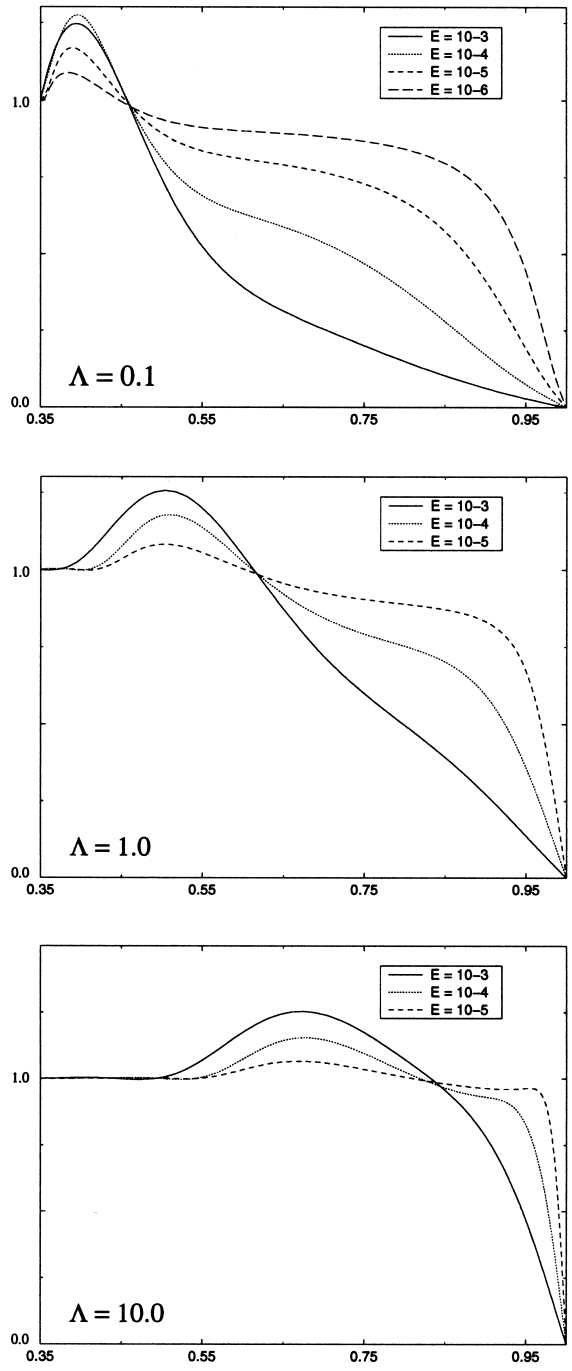

Fig. 18. Equatorial section of the angular velocity at Elsasser numbers 0.1, 1, 10 for varying Ekman numbers. One can see on each of these graphs how the amplitude of the super-rotation is controlled by viscous effects.

structure vanishes in the magnetostrophic limit but is present for Ekman number values in the range that can be investigated in the numerical geodynamo models that are being developed.

Acknowledgements

Authors wish to thank IDRIS for allowing access to Cray machines C94 and C98 through projects 960633 and 970633. We also thank the CCR Jussieu for unlimited access to a smaller Cray computer J98, which allowed us to develop and test our code, and was very useful for smaller runs. We wish to thank Andrew Soward for enlightening discussions, Henri-Claude Nataf for many useful comments and Douglas McLean for proof-reading the text. Philippe Cardin is grateful to Paul Roberts for sharing his understanding of Hartmann boundary layer singularities. ***[RO]***

References

[1] I. Proudman, The almost-rigid rotation of viscous fluid between concentric spheres, J. Fluid Mech. 1 (1956) 505–516.
[2] K. Stewartson, On almost rigid rotations, Part 2, J. Fluid Mech. 26 (1966) 131–144.
[3] R. Hollerbach, Magnetohydrodynamic Ekman and Stewartson layers in a rotating spherical shell, Proc. R. Soc. London A 444 (1994) 333–346.
[4] N. Kleeorin, I. Rogachevskii, A. Ruzmaikin, A.M. Soward, S. Starchenko, Axisymmetric flow between differentially rotating spheres in a dipole magnetic field, J. Fluid Mech. 344 (1997) 213–244.
[5] X. Song, P.G. Richards, Seismological evidence for differential rotation of the Earth's inner core, Nature 382 (1996) 221–224.
[6] W. Su, A. Dziewonski, R. Jeanloz, Planet within a planet: rotation of the inner core of the Earth, Science 274 (1996) 1883–1887.
[7] G. Dumas, A. Leonard, A divergence-free spectral expansion method for three-dimensional flows in spherical-gap geometries, J. Comput. Phys. 111 (1994) 205–219.
[8] L. Quartapelle, M. Verri, On the spectral solution of the three-dimensional Navier–Stokes equations in spherical and cylindrical regions, Comput. Phys. Commun. 90 (1995) 1–43.
[9] P.H. Roberts, On the thermal instability of a rotating fluid sphere containing heat sources, Philos. Trans. R. Soc. London A 263 (1968) 93–117.

[10] H.P. Greenspan, The Theory of Rotating Fluids, Cambridge University Press, Cambridge, 1969, 325 pp.
[11] P. Morse, H. Feshbach, Methods of Theoretical Physics, McGraw-Hill, New York, 1953, 1978 pp.
[12] R. Hollerbach, The influence of an axial field on magnetohydrodynamic Ekman and Stewartson layers, in the presence of a finitely conducting inner core, Acta Astron. Geophys. Univ. Comenianae XIX (1997) 263–275.
[13] D.J. Acheson, R. Hide, Hydromagnetics of rotating fluids, Rep. Prog. Phys. 36 (1973) 159–221.
[14] P.H. Roberts, Singularities of Hartmann layers, Proc. R. Soc. London A 300 (1967) 94–107.
[15] R. Moreau, Magnetohydrodynamics, Kluwer, Dordrecht, 1990, 313 pp.